Supporting Information

DNA Manipulation and Separation in Sub-Lithographic Scale Nanowire Array

Takao Yasui[a]*, *Sakon Rahong*[b], *Koki Motoyama*[a], *Takeshi Yanagida*[b]*, *Qiong Wu*[a], *Noritada Kaji*[a], *Masaki Kanai*[b], *Kentaro Doi*[c], *Kazuki Nagashima*[b], *Manabu Tokeshi*[a,d], *Masateru Taniguchi*[b], *Satoyuki Kawano*[c], *Tomoji Kawai*[b]*, *and Yoshinobu Baba*[a,e]*

[a]Department of Applied Chemistry, Graduate School of Engineering, Nagoya University, and FIRST Research Center for Innovative Nanobiodevices, Nagoya University, Furo-cho, Chikusa-ku, Nagoya 464-8603, Japan

[b]Institute of Scientific and Industrial Research, Osaka University, 8-1 Mihogaoka Ibaraki Osaka 567-0047, Japan

[c]Department of Mechanical Science and Bioengineering, Graduate School of Engineering Science, Osaka University, Machikaneyama-cho 1-3, Toyonaka, Osaka 560-8531, Japan

[d]Division of Biotechnology and Macromolecular Chemistry, Faculty of Engineering, Hokkaido University, Kita 13 Nishi 8, Kita-ku, Sapporo 060-8628, Japan

[e]Health Research Institute, National Institute of Advanced Industrial Science and Technology

(AIST), Takamatsu 761-0395, Japan

Dielectric breakdown of Si substrate with the 60 nm thick SiO_2 layer

Figure S1 shows photographs of (a) a fabricated Si-PDMS chip and (b) a fabricated Si-glass chip with the nanowires embedded in the microchannel. When electric voltages were applied to these fabricated chips, dielectric breakdown of the Si substrate was observed as shown in Figure S1c.

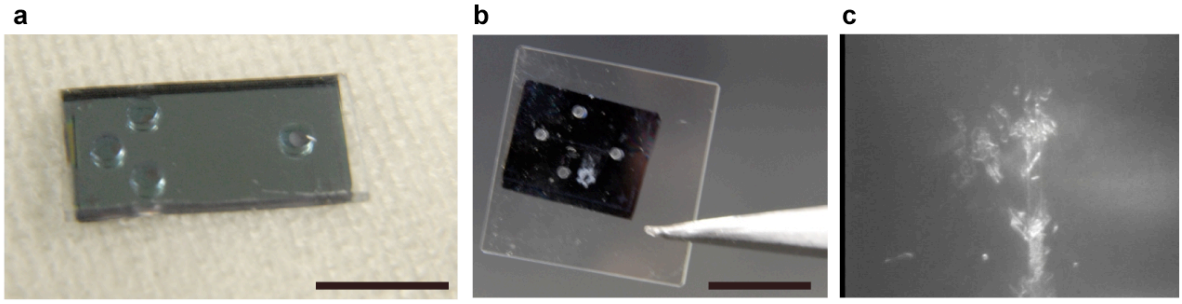

Figure S1. Photographs of (a) a fabricated Si-PDMS chip and (b) a fabricated Si-glass chip with the nanowires embedded in the microchannel; scale bar, 1 cm. (c) Micrograph of the fabricated nanowire chips after dielectric breakdown of Si substrate.

Theoretical analysis of the relaxation data

Figure S2a shows the DNA length data of five individual molecules at an arbitrary time in the nanowire spot-array structure and 1% agarose gel. These data were used to analyze the effect of nanowires and 1% agarose on the relaxation process of DNA molecules quantitatively. The dotted lines are fitting lines to data points of decaying exponentials. Many of the observable static properties of polymers in dilute solutions are well described by scaling relations. If A is an observable quantity, then $A \sim M^{\nu} \sim L^{\nu}$, where M and L are the molecular weight and length of the polymer and ν is the scaling exponent. The value of ν is independent of the local molecular structure of the polymer but does depend on temperature and monomer-solvent interactions. De Gennes proposed that these scaling laws could be generalized to dynamical properties such as relaxation and elongation rates.[1,2] In measurements of birefringence of bulk samples,[3,4] it was found that $\tau \sim \eta L^{1.5}/k_B T$, where τ is the relaxation time, η is the viscosity of the solvent, k_B is the Boltzmann constant, and T is the absolute temperature, and therefore, the scaling exponent is $3\nu = 1.5$, in accordance with the Zimm model for a Θ-solvent, in which monomer-monomer interactions are canceled by monomer-solvent interactions.[5,6] This result was independent of the quality of the solvent as it was varied from a Θ-solvent ($3\nu = 1.5$) to a good solvent ($3\nu = 1.8$), where there is net swelling of the polymer relative to the Θ-solvent. This apparent suppression of excluded volume effects contradicts the theoretical predicted scaling exponent of $3\nu = 1.8$,[7] which has been observed in intrinsic viscosity measurements. However, the relation between birefringence and extension is not entirely clear because it requires independent knowledge of the polarizability and chain conformation. In terms of relaxation scaling exponents, the measured exponent is about $3\nu = 1.65$ for good solvents,[8-12] instead of the theoretical value of $3\nu = 1.8$.

The relaxation times follow a scaling law with chain length $\tau \sim L^{3\nu}$ (Figure S2b). The relaxation-scaling exponent, 3ν, 1.6 ± 0.1 and 2.0 ± 0.1 in the nanowire spot-array structure and the 1% agarose gel, respectively, gives the best fit to the experimental value. In reported works,[13,14] the quantitative values for relaxation of a single DNA molecule were 1.7 ± 0.1 and 2.0 ± 0.2 for the relaxation-scaling exponent in free solution and polymer (semi-dilute) solution, respectively. The value for the relaxation-scaling exponent in the 1% agarose gel, 2.0 ± 0.1, showed a good correspondence to that in polymer solution, 2.0 ± 0.2, and we could conclude that our experimental data were well able to express the kind of solution that DNA molecules are in. We found that the value for the relaxation-scaling exponent in the nanowire spot-array structure, 1.6 ± 0.1, showed a good agreement with that in the free solution, 1.7 ± 0.1, and therefore, DNA molecules showed free-solution-like dynamics inside the nanowire spot-array structure. Considering only 2% as the volume fraction of nanowires within the microchannel, it also made sense that DNA molecules in the nanowire spot-array structure showed the free-solution-like relaxation dynamics. These results highlighted that the DNA elongation events within the nanowire spot-array structure were mainly due to an entanglement with nanowires, whereas the DNA contraction might be governed by the outside the nanowire spot-array structure (low nanowire density area).

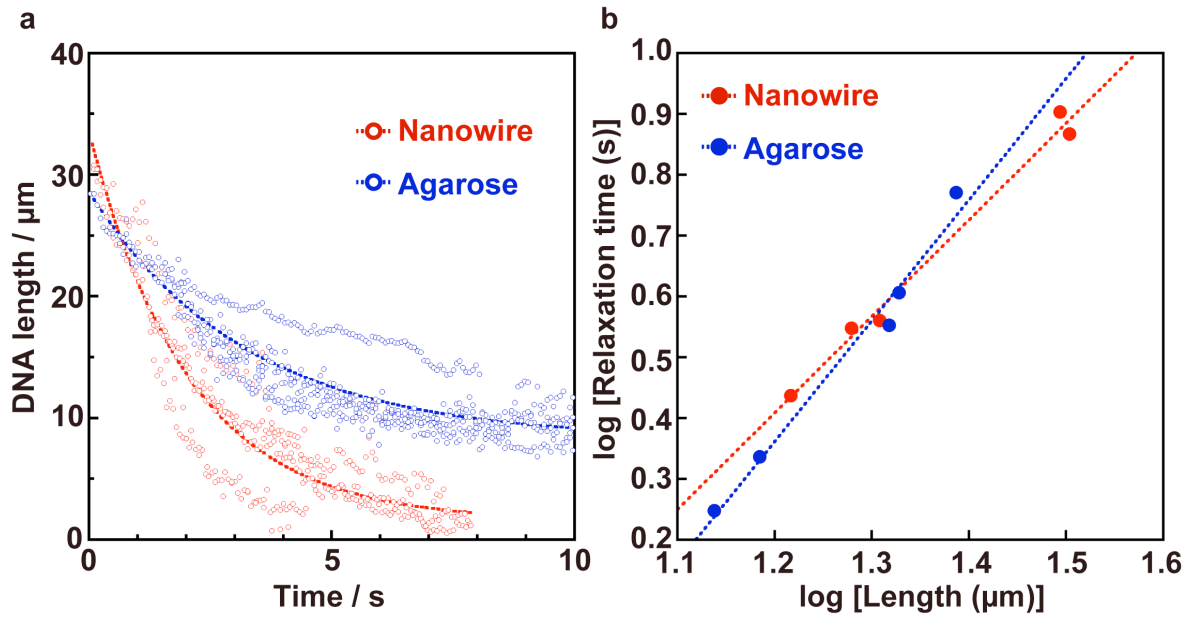

Figure S2. (a) Plot of T4-DNA length in response to time for the relaxation process of the T4-DNA molecule in the nanowire spot-array structure (red circles) and in the 1% agarose gel (blue circles). The dotted lines are decaying exponentials fitted to data points. (b) Scaling of the relaxation time with length in the nanowire spot-array structure (red circles) and the 1% agarose gel (blue circles). The dotted lines are linear fits to data points and they yielded slopes of 1.6 ± 0.1 and 2.0 ± 0.1 in the nanowire spot-array and the 1% agarose gel, respectively. These fits demonstrated dynamical scaling of the relaxation time, τ, with length and these slopes showed relaxation-scaling exponents.

Electric field calculation for the nanowire array

Electric fields near nanopillars (and nanowires) can be evaluated by solving the Poisson equation and the Laplace equation with the appropriate boundary conditions. In addition, the Nernst-Planck equation is also solved to take into account the distribution of the electrolyte ions which cover the surface. The surface charges of nanopillars (and nanowires) are screened by the electric double layer due to the high concentration of electrolyte. Figure S3 shows a schematic of the boundary conditions around the nanopillar (and nanowire). The electric double layer is formed in the region of $a \le r < b$ and the dielectric boundary condition is satisfied at $r = b$. The voltage of the surface V_0 is defined at $r = a$. In this study, a two-dimensional theoretical model is developed. Therefore, the existence of line charges is assumed at $r < a$. The electrostatic potential at $a \le r < b$, considering the electric double layer, can be represented by the Poisson equation as follows:

$$-\varepsilon_i \Delta V_i(r,\varphi) = q_a + zen(r), \quad a \le r < b, \tag{S1}$$

where V_i is the electrostatic potential, ε_i is the permittivity, q_a is the line charge in the nanopillar (and nanowire), z and $n(r)$ are the valence and the number distribution of the electrolyte, respectively, and e is the elementary charge. In this region, it is acceptable that $n(r)$ can be represented only by r and is independent of ϕ. Therefore, V_i is also a function of r and independent of ϕ. Consequently, the electric field $E(r)$ can be expressed as follows:

$$E(r) = -\nabla V_i(r) = \frac{1}{2\pi\varepsilon_i r}\left(Q_a + Q(r)\right), \quad a \le r < b, \tag{S2}$$

where $Q_a = 2\pi a q_a$ and $Q(r) = 2\pi\int_a^r n(r) r dr$. The distribution $n(r)$ of electrolyte is determined based on the steady state of the Nernst-Planck equation:

$$-D\nabla n(r) - \frac{1}{\xi}\nabla V_i(r) Q(r) = 0, \tag{S3}$$

where D is the diffusion coefficient and ξ is the friction coefficient. Substituting Eq. (S2) into Eq. (S3) gives $V_i(r)$ according to the boundary condition of $V_i(a) = V_0$, such that

$$V_i(r) = -\frac{Q_a}{2\pi\varepsilon_i}\ln\frac{r}{a} - \frac{1}{2\pi\varepsilon_i}\int_a^r \frac{Q(r')}{r'} dr' + V_0 . \tag{S4}$$

On the other hand, the electric field of $E(r)$ must be uniform at the limit of $r \to \infty$. Then, $E(r)$ is represented as follows:

$$V_o(r) = E(r-b)\cos\varphi + E\left(\frac{b^2}{r} - b\right)\cos\varphi - \frac{Q_a}{2\pi\varepsilon_o}\frac{1}{1-\gamma(b/a)^{\xi}}\ln\frac{r}{b}, \quad r \ge b, \tag{S5}$$

where the boundary conditions

$$\varepsilon_o\frac{\partial V_o}{\partial r} = \varepsilon_i\frac{\partial V_i}{\partial r} \quad \text{and} \quad V_o(b) = 0 \tag{S6}$$

are adopted, γ is the parameter determined from the normalization constant of $Q(r)$, and ζ is the

constant with respect to the Coulomb energy and the thermal fluctuation. The theoretical details will be described elsewhere (manuscript in preparation).

According to Eqs. (S4) and (S5), the electric field near the nanowire is obtained as shown in Figures S4 and S5. In this case, the parameters are set as: a = 5 nm, b = 6 nm, Q_a = -1.0×10^{-11} C/m; and the temperature is 293 K. The permittivity of buffer solution is set to the same value as water at 293 K, 80.1, regardless of the concentration of electrolyte. The surface voltage of the nanowire is V_0 = -20 mV according to the experimental result. It is found that $E(r)$ near the surface becomes weaker due to the screening effect by the electrolyte solution. Outside the electric double layer, $E(r)$ becomes uniform. On the other hand, Figure S6 shows the results for a = 50 nm, b = 51 nm, Q_a = -1.0×10^{-10} C/m. In this case, screening of the surface charges appears to be affected more broadly than in the first case. Figure S7 shows the results from the post-array of 10 nm diameter nanowires. Assuming interactions between the nanowires are very weak, $E(r)$ is evaluated from the simple sum of the electric field around the single wire. It is found that $E(r)$ near the assembly of nanowires is a stronger field than that around the large single pillar. The surface charges are sufficiently screened so that the external electric field seems to penetrate the post-array. It is suggested that the post-array of nanowires, which are fabricated in a bottom-up process, critically affects the different behavior characteristics of DNA.

Comparison of the distributions for the nanowire spot-array structure with that for the nanopillar structure revealed that the electric fields within the small nanowire spot-array are larger than those around the large nanopillar. Therefore in principle DNA molecules can easily enter and collide with the nanowire spot-array structure more frequently than the nanopillar structure, which enhances the elongation of DNA molecules within the nanowire post-array structure. When comparing the electric field distributions for one nanowire (10 nm in diameter) and nanopillar (100 nm in diameter) in the same x-y plane, the electric field for smaller nanowires increases more rapidly with increasing distance from the center of the nanowire. Both of the electric fields converge to the external uniform field of 10 V/cm. Differences in the peculiar electric field near the nanostructures are caused by the boundary conditions determined from their geometries, charges, and surface voltages. As a result, the electric field near the nanowire converges more rapidly than that of the larger nanopillar. In other words, DNA molecules do not feel the electrostatic fields from the nanowires so sensitively, although the spot-array disturbs the flow dynamics physically. Thus these theoretical calculations highlight that the smaller nanowire spot-array structure can increase the frequency of DNA collisions compared to the larger nanopillar structure due to modifications of the electric field within the spot-array.

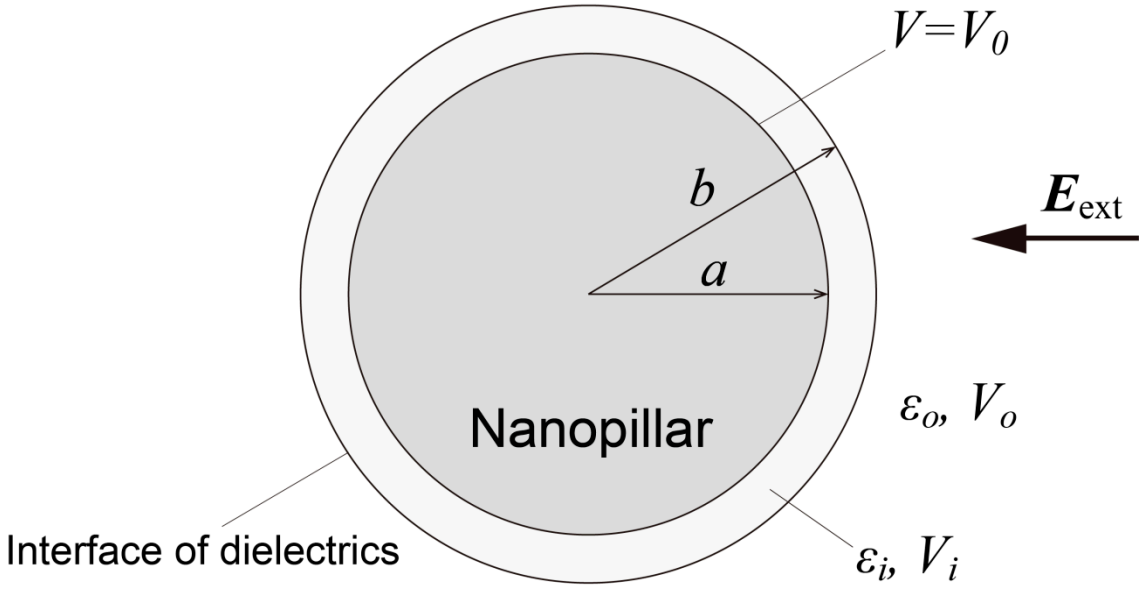

Figure S3. Schematic illustration of a nanopillar (and nanowire) in a uniform electric field and the boundary conditions.

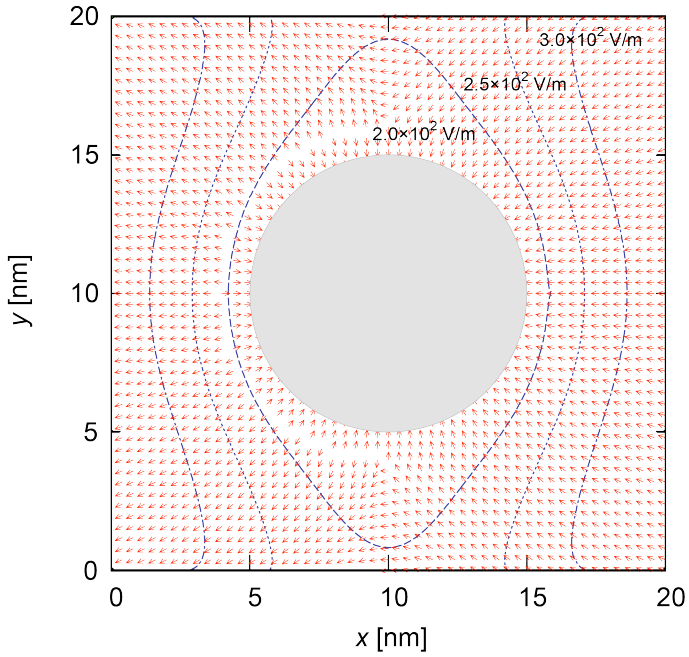

Figure S4. Electric field presented by red-colored vectors near the 10 nm diameter nanowire located at $(x,y) = (10,10)$ in the uniform electric field of $E_x = -1.0 \times 10^3$ V/m. Dashed, dotted, and chain contour lines correspond to values of 2.0×10^2, 2.5×10^2, and 3.0×10^2 V/m, respectively.

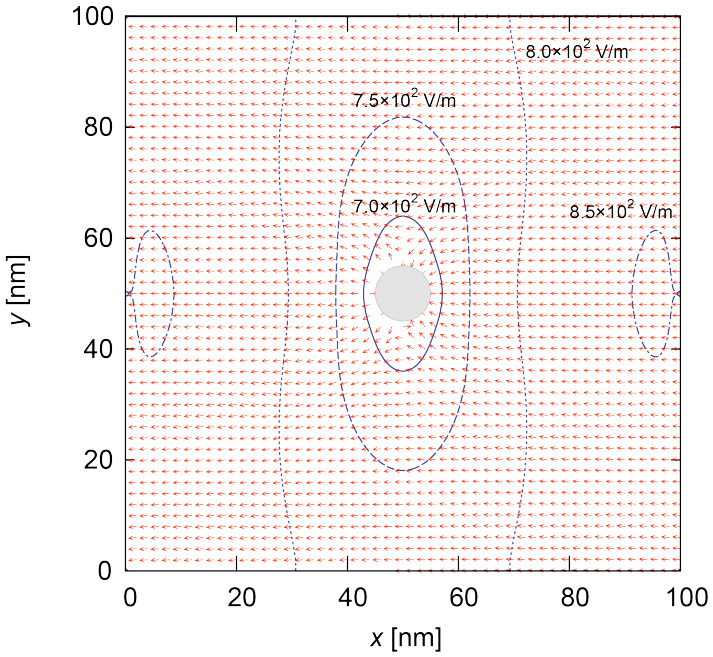

Figure S5. Electric field presented by red-colored vectors near the 10 nm diameter nanowire located at $(x,y) = (50,50)$ in the uniform electric field of $E_x = -1.0 \times 10^3$ V/m. Solid, dashed, dotted, and chain contour lines correspond to values of 7.0×10^2, 7.5×10^2, 8.0×10^2, and 8.5×10^2 V/m, respectively.

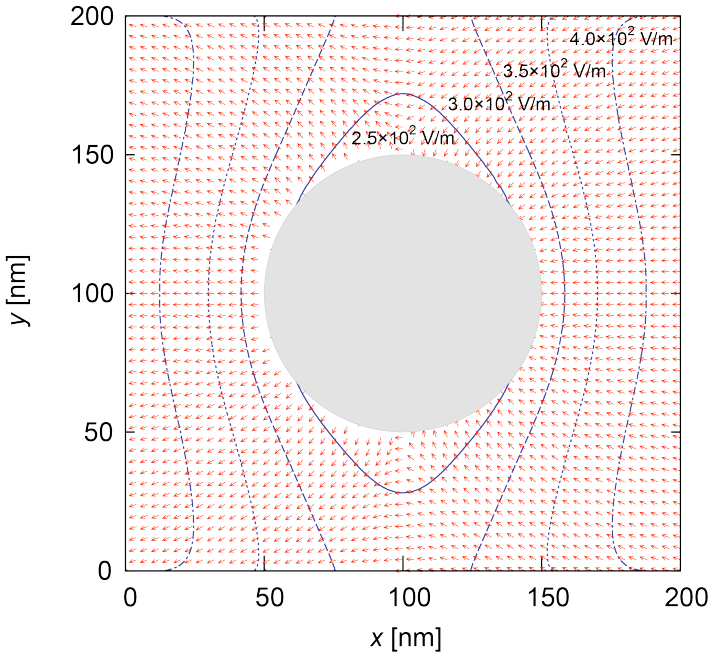

Figure S6. Electric field presented by red-colored vectors near the 100 nm diameter nanopillar located at $(x,y) = (100,100)$ in the uniform electric field of $E_x = -1.0 \times 10^3$ V/m. Solid, dashed, dotted, and chain contour lines correspond to values of 2.5×10^2, 3.0×10^2, 3.5×10^2, and 4.0×10^2 V/m, respectively.

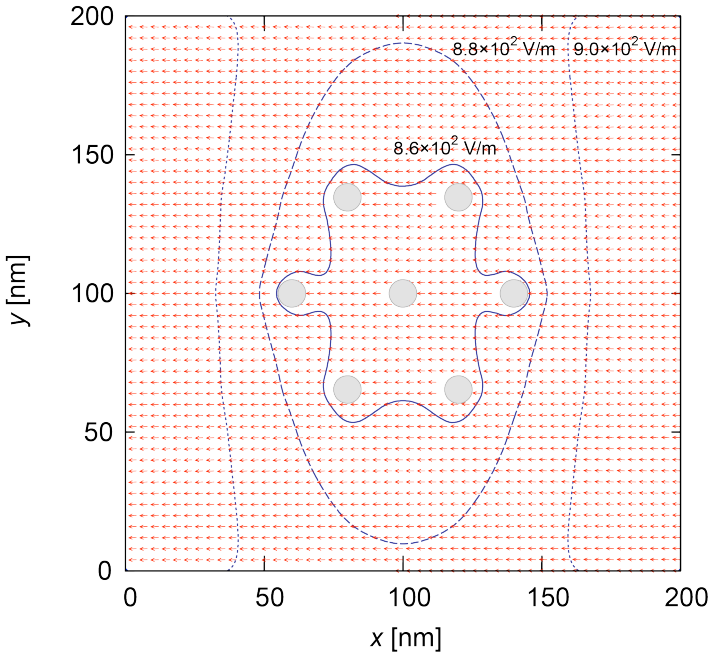

Figure S7. Electric field presented by red-colored vectors near the nanowire post-array in the uniform electric field of E_x = -1.0 × 10^3 V/m. Solid, dashed, dotted, and chain contour lines correspond to values of 8.6 × 10^2, 8.8 × 10^2, 9.0 × 10^2, respectively.

Nanowires embedded in the nanopore channel

Figure S8 shows a schematic of the fabricated chip and FESEM images of the nanowires embedded in the nanopore channel. The nanowire position is well controlled and the fabricated nanowires are only self-assembled in the microchannel adjacent to the nanopore channel.

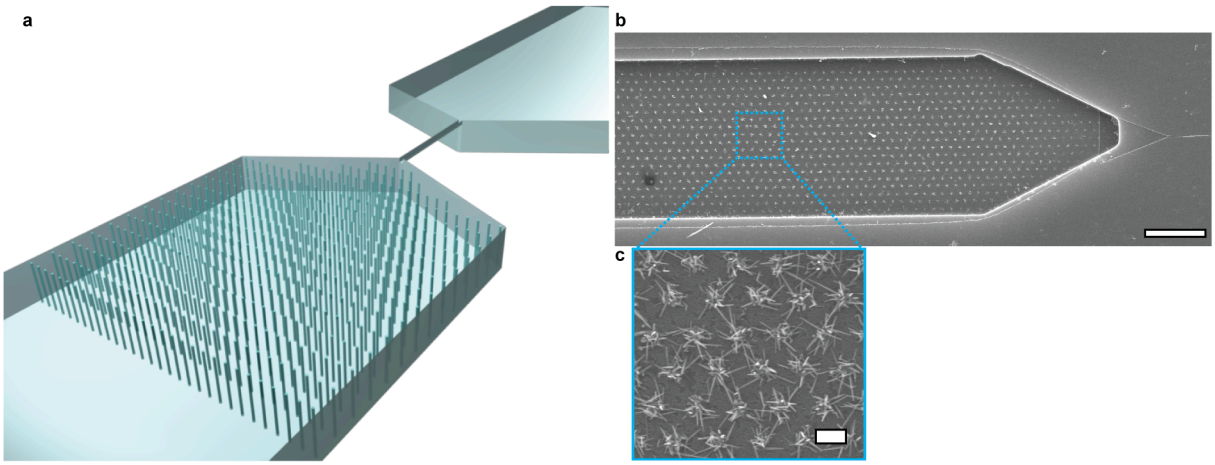

Figure S8. (a) Schematic of fabricated chip. (b) FESEM image of the fabricated nanowires embedded nanopore channel; scale bar, 10 μm. (c) Magnified FESEM image of the fabricated nanowires embedded nanopore channel; scale bar, 1 μm.

Movies

Movie 1. Migration of a single T4-DNA molecule in the nanowire spot-array structure.

Movie 2. Migration of a single T4-DNA molecule in the nanowire spot-array structure with an "M" shaped conformation.

Movie 3. Migration of a single T4-DNA molecule in the nanowall array structure.

Movie 4. Relaxation process of a single T4-DNA molecule in the nanowire spot-array structure.

References

1. de Gennes, P. G., Dynamics of Entangled Polymer-Solutions .2. Inclusion of Hydrodynamic Interactions. *Macromolecules* **1976,** *9*, 594-598.
2. de Gennes, P. G., Dynamics of Entangled Polymer-Solutions .1. Rouse Model. *Macromolecules* **1976,** *9*, 587-593.
3. Keller, A.; Odell, J. A., The Extensibility of Macromolecules in Solution - a New Focus for Macromolecular Science. *Colloid. Polym. Sci.* **1985,** *263*, 181-201.
4. Narh, K. A.; Odell, J. A.; Keller, A., Temperature-Dependence of the Conformational Relaxation-Time of Polymer-Molecules in Elongational Flow - Invariance of the Molecular-Weight Exponent. *J. Polym. Sci., Part B: Polym. Phys.* **1992,** *30*, 335-340.
5. Rouse, P. E., A Theory of the Linear Viscoelastic Properties of Dilute Solutions of Coiling Polymers. *J. Chem. Phys.* **1953,** *21*, 1272-1280.
6. Zimm, B. H., Dynamics of Polymer Molecules in Dilute Solution - Viscoelasticity, Flow Birefringence and Dielectric Loss. *J. Chem. Phys.* **1956,** *24*, 269-278.
7. Doi, M.; Edwards, S. F., *The Theory of Polymer Dynamics*. Oxford University Press, USA: 1988; Vol. 73.
8. Adam, M.; Delsanti, M., Light-Scattering by Dilute-Solution of Polystyrene in a Good Solvent. *J. Phys.* **1976,** *37*, 1045-1049.
9. Adam, M.; Delsanti, M., Dynamical Properties of Polymer-Solutions in Good Solvent by Rayleigh-Scattering Experiments. *Macromolecules* **1977,** *10*, 1229-1237.
10. Tsunashima, Y.; Nemoto, N.; Kurata, M., Dynamic Light-Scattering-Studies of Polymer-Solutions .1. Histogram Analysis of Internal Motions. *Macromolecules* **1983,** *16*, 584-589.
11. Tsunashima, Y.; Nemoto, N.; Kurata, M., Dynamic Light-Scattering-Studies of Polymer-Solutions .2. Translational Diffusion and Intramolecular Motions of Polystyrene in Dilute-Solutions at the Theta-Temperature. *Macromolecules* **1983,** *16*, 1184-1188.
12. Nemoto, N.; Makita, Y.; Tsunashima, Y.; Kurata, M., Dynamic Light-Scattering-Studies of Polymer-Solutions .3. Translational Diffusion and Internal Motion of High Molecular-Weight Polystyrenes in Benzene at Infinite Dilution. *Macromolecules* **1984,** *17*, 425-430.
13. Perkins, T. T.; Quake, S. R.; Smith, D. E.; Chu, S., Relaxation of a Single DNA Molecule Observed by Optical Microscopy. *Science* **1994,** *264*, 822-826.
14. Ferree, S.; Blanch, H. W., The Hydrodynamics of DNA Electrophoretic Stretch and Relaxation in a Polymer Solution. *Biophys. J.* **2004,** *87*, 468-475.